International Journal for Housing Science and Its Applications
Publish August 6, 2025. Volume 46, Issue 3 Pages 8285-8295

https,//doi.org/10.70517/ijhsa463708

Improvement of regulation accuracy of motorized bus frequency based on adaptive fuzzy control algorithm

Yixing Bao[1,*]
[1] Department of Data and Systems Engineering, The University of Hong Kong, Hong Kong, 999077, China
Corresponding authors: (e-mail: sjmy4046@connect.hku.hk).

Abstract The frequency regulation accuracy of electric bus directly affects power system stability and security. In this study, the physical model of electric busbar is established, and the PSO-ANFIS control model is constructed by combining adaptive neuro-fuzzy inference system (ANFIS) and improved particle swarm optimization algorithm (PSO). The model adopts the Sugeno fuzzy system as the basic framework, extracts the complex mapping relations in the training samples using subtractive clustering method, and optimizes the ANFIS parameters by the improved PSO algorithm to improve the model generalization and accuracy. Experimental validation shows that the method can realize the precise adjustment of output frequency accuracy in the order of 0.8E-12 when the frequency control word variation is 192315 times the minimum step value. Comparative analysis of multi-region simulation shows that compared with the traditional PI control and centralized model predictive control, the PSO-ANFIS model improves the frequency deviation regulation level in region 1 by 56.85% and 26.54%, and improves the regional control deviation (ACE) regulation by 50.56% and 40.54%, respectively. In addition, when coordinating fixed-frequency and variable-frequency electric buses to participate in regulation together, the maximum frequency deviation of the system is reduced to -0.1236 Hz, and the power deviation of the contact line is reduced to 0.0267 p.u., which is significantly better than that of a single type of electric bus participating in regulation. The study shows that the proposed adaptive fuzzy control algorithm can effectively improve the regulation accuracy of the electric bus frequency, accelerate the frequency recovery speed, reduce the overshooting amount of the FM, and better coordinate the contact line power fluctuation of the multi-area power system.

Index Terms Adaptive fuzzy control, Electric bus, Frequency regulation accuracy, Particle swarm optimization, Neuro-fuzzy inference system

I. Introduction

Accompanied by the vigorous promotion of energy saving and emission reduction policies, the new energy industry has developed rapidly, and new energy vehicles, as one of the key development directions, have faced many design challenges [1]. As a new energy vehicle power source, the new energy electric drive system replaces the fuel engine on the traditional automobile, and the rationality and reliability of its design affects the performance and service life of the whole vehicle [2]. The main role of the motor controller is to convert the bus battery DC inverter into three-phase AC power required to drive the motor, in the vehicle layout environment of the battery connected to the motor controller wiring harness is longer, resulting in a larger inductance on this section of the wiring harness, the battery can not respond quickly to the motor controller power device high-frequency switching load current demand changes, therefore, in the motor controller needs to be paralleled with a bus capacitor [3]-[5]. The main role of the bus capacitor is to smooth the bus voltage to weaken the bus voltage spikes and absorb the ripple current, with which the three key parameters of the bus capacitor are bus capacitance, equivalent series inductance ESL, and equivalent series resistance ESR [6]-[8]. Among them, the equivalent series resistance ESR reflects the capacitor's ability to withstand ripple current, which refers to the high-frequency current flowing through the bus capacitor, and the ripple current is too large to cause the bus capacitor to heat up, which directly affects the capacitor's life [9], [10].

In the current electric vehicle high-voltage DC system integration process, the modules are often individually designed and then simply interconnected through the DC bus, ignoring the coupling between the modules [11]. Although the source/carrier-side modules can work stably individually, the integrated system may experience bus instability [12]. This is due to the fact that power electronic converters with strict closed-loop control and the loads they carry have constant power characteristics, while constant power loads (CPLs) embody negative impedance characteristics, which directly lead to a reduction in the stability of the system [13]-[15]. When the DC bus destabilization occurs, the bus voltage will oscillate significantly beyond the normal fluctuation range, which can

easily trigger the circuit protection device action, and in serious cases, even lead to system collapse [16], [17]. Through the failure data statistics of a domestic electric vehicle, it is found that the failure ratio of its high-voltage system is more than 80%, which is far more than the failure ratio of other systems [18]. Therefore, from the perspective of the system to analyze the stability of the DC bus frequency of the high-voltage system of electric vehicles, to clarify the limitations on the access load, and on this basis, research and propose the method of regulating the electric bus frequency is of great significance to reduce the high-voltage system failure and to ensure the safe driving of the whole vehicle.

The safe and stable operation of the power system depends on the precise control of the system frequency, and the frequency regulation accuracy of the motorized busbar, as an important infrastructure in the power system, directly affects the operation quality of the whole system. Currently, the power system is facing challenges such as complex structure, diverse loads and variable operation modes, and the traditional frequency control methods often show insufficient regulation accuracy, slow response speed and unstable regulation effect when dealing with large disturbances and nonlinear situations. Especially in the context of high proportion of new energy access, the frequency stabilization of the power system becomes more complex due to the intermittent and fluctuating characteristics of new energy sources such as wind power and photovoltaic. At the same time, in the multi-regional interconnected power system, frequency regulation not only needs to consider the frequency restoration in a single region, but also needs to coordinate the power balance between regions, which puts forward higher requirements for frequency regulation technology. In recent years, intelligent control algorithms have shown great potential in the field of power system frequency regulation, among which adaptive fuzzy control has become a research hotspot due to its ability to effectively deal with system uncertainty and nonlinear problems. However, the existing adaptive fuzzy control methods still have room for improvement in terms of parameter optimization, system robustness and multi-region coordination. Especially under the demand of high-precision frequency regulation, how to integrate advanced optimization algorithms in order to improve the accuracy and adaptability of fuzzy control has become an urgent problem to be solved. In addition, considering the special role of electric bus in frequency regulation, how to design a specialized control strategy for its physical characteristics and realize multi-region coordinated frequency regulation on this basis is also an important direction of current research. In view of the above problems, this paper proposes an adaptive fuzzy control algorithm based on PSO-ANFIS to improve the frequency regulation accuracy of electric busbar. The study first establishes the physical mathematical model of the electric bus, and provides a theoretical basis for the subsequent design of the control strategy by analyzing its mechanical response characteristics. Then, the control framework based on adaptive neuro-fuzzy inference system is constructed, and the parameters of ANFIS are optimized by combining with the improved particle swarm optimization algorithm to improve the adaptive ability and control accuracy of the system. The study adopts the Sugeno fuzzy system as the infrastructure, and utilizes the subtractive clustering method to extract the complex mapping relationships in the training samples to effectively deal with nonlinear and big data problems. Meanwhile, the global search ability and convergence efficiency of the algorithm are enhanced by improving the inertia weight updating strategy and particle stagnation processing mechanism in the particle swarm algorithm. On this basis, a coordinated control strategy for multi-area power systems is designed to realize the cooperative participation of fixed-frequency electric bus and inverter electric bus in frequency regulation. Through simulation analysis and experimental verification, the performance of the proposed method is comprehensively evaluated in different scenarios and compared with the traditional control method to verify its advantages in frequency regulation accuracy, response speed and system stability.

II. Adaptive fuzzy control algorithm

II. A. Modeling framework

Solving the deflection of a busbar by means of physical parameters, geometrical size, boundary conditions and load cases of an electric busbar is a classical problem in plate and shell theory, and there are already mature analytical methods, including the mechanical response of the busbar under load forms such as uniform load and centralized load [19]. In this study, the centralized load is chosen as a calculation sample:

$$f_1(\lambda, F, (x_F, y_F), pw) = 0 \tag{1}$$

where, p is the operator of the differential operator function, λ is the own physical parameters such as the modulus of elasticity of the motorized busbar, F, x_F, y_F is the centralized loading case, and w is the deflection function of the busbar.

For Eq. (1), the boundary conditions are given as:

$$w|_{\partial\Omega} = w_0, pw|_{\partial\Omega} = pw_0 \tag{2}$$

where $\partial\Omega$ is the boundary.

The deflection function is obtained through Eqs. (1) to (2), which in turn solves for the other mechanical responses of the motorized busbar.

In the inverse problem, the loading case of the busbar is solved by the physical parameters, geometric size, boundary conditions and deflection of the motorized busbar as:

$$(F,(x_F,y_F)) = f_2(\lambda, pw) \tag{3}$$

II. B.PSO-ANFIS modeling

II. B. 1) Adaptive neuro-fuzzy control systems

Adaptive Neuro-Fuzzy Inference System (ANFIS) is a new fuzzy inference system for fuzzy models [20]. It is based on neural network and integrates three parts of fuzzy system, namely fuzzification, fuzzy inference and defuzzification, and is able to adaptively learn and generate if-then inference rules. A hybrid algorithm of backpropagation algorithm + least squares estimation is selected for model parameter optimization. For ease of understanding, the two-input classical ANFIS model is used in this study for introduction. Figure 1 shows the structure of the ANFIS model, which is a network with a 5-layer structure containing 2 input layers and 1 output layer, and also contains 2 if-then inference rules for the TS fuzzy model. Square nodes represent that the parameters of the node are adjustable and round nodes represent that the parameters of the node are not adjustable. Each layer of nodes has a similar function, and the output data of the nodes in the previous layer will be used as the input data of the nodes in the next layer.

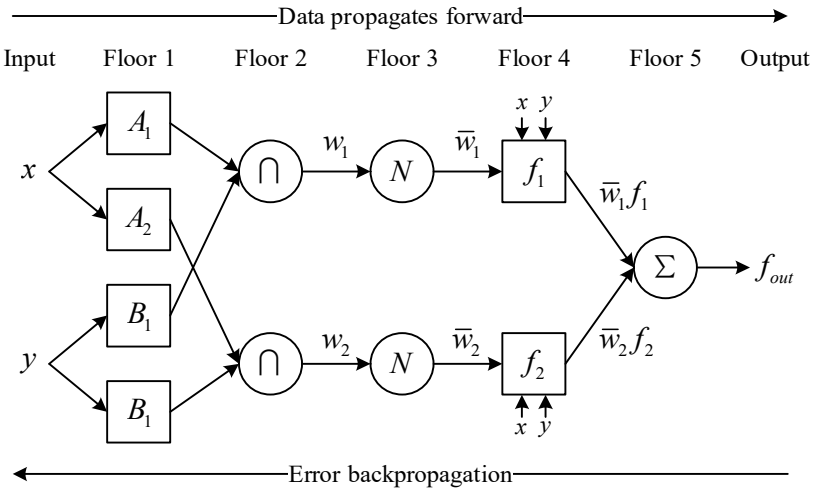

Figure 1: Structure of the ANFIS model

In ANFIS model, x, y is the input and f_{out} is the output. The nodes in layer 15 are calculated by the formulae respectively:

$$\begin{cases} O_{1,i} = \mu A_i(x) = \dfrac{1}{1+\left[\left(\dfrac{x-c_i}{a_i}\right)^2\right]^{b_i}} \\ O_{1,i} = \mu B_i(y) = \dfrac{1}{1+\left[\left(\dfrac{y-c_i}{a_i}\right)^2\right]^{b_i}} \end{cases} \tag{4}$$

$$O_{2,j} = \mu A_i(x) \cdot \mu B_i(y) = w_i, i = 1,2 \tag{5}$$

$$O_{3,j} = \frac{w_i}{\sum w_i} = \frac{w_i}{w_i + w,} = \overline{w_i}, i = 1,2 \tag{6}$$

$$O_{4j} = \overline{w_i} f_i == \overline{w_i}(r_i + p_i x_1 + q_i x_2), i = 1,2 \tag{7}$$

$$O_{5j} = \sum_i \overline{w_i} f_i = \frac{\sum_i w_i f_i}{\sum_i w_i} = f_{out} \tag{8}$$

The fuzzy inference rules R_1 and R_2 of the system can be formulated as follows:

$$R_1 : \text{If } x \text{ is } A_1 \text{ and } y \text{ is } B_1, \text{then } f_1 = p_1 x + q_1 y + r_1 \tag{9}$$

$$R_2 : \text{If } x \text{ is } A_2 \text{ and } y \text{ is } B_2, \text{then } f_2 = p_2 x + q_2 y + r_2 \tag{10}$$

Parameters $\{p_i, q_i, r_i\}$ and $\{a_i, b_i, c_i\}$ in the system are trained using the LSE method and BP algorithm, respectively, and they will be continuously self-optimized during the training process to achieve adaptive learning of the system.

II. B. 2) Sugeno modeling system

In fuzzy systems, Mamdani model and Sugeno model are often used. In this study, Sugeno model system is chosen, whose typical fuzzy rule is if-then rule, i.e.:

$$\text{If } x \text{ is } A \text{ and } y \text{ is } B, \text{then } z = f(x, y) \tag{11}$$

where, A, B is the fuzzy set in the antecedent and $z = f(x, y)$ is the exact function in the consequent. If $f(x, y)$ is a linear function, the resulting system is a 1st order Sugeno-type fuzzy system.

It is specified that - a 1st order Sugeno-type fuzzy system structure contains 2 fuzzy rules:

$$\text{If } x \text{ is } A_1 \text{ and } y \text{ is } B_1, \text{then } f_1 = p_1 x + q_1 y + r_1 \tag{12}$$

$$\text{If } x \text{ is } A_2 \text{ and } y \text{ is } B_2, \text{then } f_2 = p_2 x + q_2 y + r_2 \tag{13}$$

where, x, y is the input, A_1, B_1, A_2, B_2 is the generalized language in the fuzzy system, f_1, f_2 is the output of the fuzzy system and $\{p_i, q_i, r_i\}(i = 1,2,\cdots)$ is the set of conclusion parameters of the fuzzy system.

Layer 1 is the input layer and its main role is to utilize the positive problem data as training samples:

$$O_i^1 = \mu A_i(x) \quad (i = 1,2) \tag{14}$$

$$O_j^1 = \mu B_j(y) \quad (j = 1,2) \tag{15}$$

where, O_i^1, O_j^1 is the affiliation of the input layer and $\mu A_i(x), \mu B_j(y)$ is the affiliation function of each input layer. The bell-type function is chosen for this study, Eq:

$$\mu A_i(x) = \frac{1}{1 + \left| \frac{x - c_{A_i}}{a_{A_i}} \right|^{2b_{A_i}}} \quad (i = 1,2) \tag{16}$$

$$\mu B_i(y) = \frac{1}{1 + \left| \frac{y - c_{B_j}}{a_{B_j}} \right|^{2b_{B_j}}} \quad (j = 1,2) \tag{17}$$

where $a_{A_i}, b_{A_i}, c_{A_i} (i = 1,2)$ and $a_{B_j}, b_{B_j}, c_{B_j} (j = 1,2)$ are both premise parameters.

Layer 2 is the fuzzy rule layer, whose main role is to compute the fitness of the rule from all the input signals:

$$O_i^2 = \omega_i = \mu A_i(x) \cdot \mu B_j(y) \quad (i, j = 1,2) \tag{18}$$

where, O_i^2 is the adaptation value of an abstract rule in this system and ω_i is the incentive strength of an abstract rule in this system.

Layer 3 is the normalization layer and its main role is to normalize the adaptation degree:

$$O_i^3 = \overline{\omega_l} = \frac{\omega_i}{\sum_{i=1}^{2} \omega_i} \quad (i = 1,2) \tag{19}$$

where, O_i^3 is the normalized applicability value corresponding to a particular abstract rule in the system, $\overline{\omega_l}$ is the applicability percentage corresponding to a particular abstract rule in the system.

Layer 4 is the computational output layer, whose main role is to compute the output results of each rule:

$$O_i^4 = \overline{\omega}_l f_i = \overline{\omega}_l (p_i x + q_i y + r_i)(i = 1,2) \tag{20}$$

where, O_i^4 is the output value before deblurring, , f_i is the structure of the fuzzy system chosen for this study.

Layer 5 is the total output layer, whose main role is to calculate the total output of the system:

$$O_i^5 = \sum_i \overline{\omega}_i f_i = \frac{\sum_i \omega_i f_i}{\sum_i \omega_i} \tag{21}$$

ANFIS has two training structures for fuzzification processing, grid classification and subtractive clustering. The fuzzification process is to extract the complex mapping relationships in the training samples in a localized way, so as to resolve the complex nonlinear and big data problems. In this study, the subtractive clustering method is selected, the basic principle of which is by solving the density of neighboring points in the space. According to the density distribution of adjacent points to determine the possibility of the center point as the center of clustering. The clustering center of the system is selected after calculating the possibility of all the points.

Then PSO is used to search for the best fitness value in ANFIS, so as to improve the superiority of the parameters in the ANFIS model, greatly reduce the influence of the initial parameters set by manual experience on the prediction results of the model, and improve the model's generalization and accuracy.

II. B. 3) Improved Particle Swarm Algorithm

Particle Swarm Optimization (PSO) algorithm was proposed by a scholar based on the foraging and pursuit avoidance behaviors of swarm animals - a global search algorithm [21]. The algorithm is robust, easy to combine with other algorithms, requires fewer parameters to be adjusted, and has profound significance for scientific research and engineering applications.

The PSO algorithm is mathematically described as a population $x = (x_1, x_2, \cdots, x_m)^T$ of m particles in a n-dimensional search space, where the i th particle has a position of $x_i = (x_{i,1}, x_{i,2}, \cdots, x_{i,n})^T$ and a velocity of $v_i = (v_{i,1}, v_{i,2}, \cdots, v_{i,n})^T$. The individual extremum is $p_i = (p_{i,1}, p_{i,2}, \cdots, p_{i,n})^T$ and the population global extremum is $p_g = (p_{g,1}, p_{g,2}, \cdots, p_{g.n})^T$. The particles update their positions and velocities according to Eq. (22) and Eq. (23) after they have found the individual and population extremum:

$$v_{i,d}^{k+1} = \rho v_{i,d}^k + c_1 rand()(p_{i,d}^k - x_{i,d}^k) + c_2 rand()(p_{g,d}^k - x_{i,d}^k) \tag{22}$$

$$x_{i,d}^{k+1} = x_{i,d}^k + v_{i,d}^{k+1} \tag{23}$$

where, c_1, c_2 - Learning factor or acceleration constant, ρ - Inertia weight, $rand()$ - Random number between (0, 1), $x_{i,d}^k, v_{i,d}^k$ - Position and velocity of particle i in the d th dimension in the k th iteration, $p_{i,d}^k$ - Position of particle i in the d th dimension at the individual pole's position, $p_{g,d}^k$ -Population's position in the d th dimension global pole.

From Eqs. (22) and (23), it can be seen that c_1 is used for the step size adjustment of the particle searching for its own optimal position, and c_2 is used for the step size adjustment of the particle searching for the global optimal position. Therefore, according to the problem demand, the inertia weights can be updated by updating the particle

in fitness to adjust the step length of the particle in the optimization process, so as to improve its global search ability. In order to guarantee the global and local search ability at the initial stage of optimization, c_1 is set as a fixed value and c_2 is linearly decreasing. The specific formula is shown below:

$$\hat{f} = \frac{\sum_{i}^{n} f_i}{n} \tag{24}$$

$$\rho(t) = \begin{cases} \rho_{\min} + \dfrac{f - f_{set}}{f_{avg}}(\rho_{\max} - \rho_{\min}), f \le f_{avg} \\ \rho_{\max}, f > f_{avg} \end{cases} \tag{25}$$

$$c_2(t) = c_{2\min} + \frac{k}{k_{\max}}(c_{2\max} - c_{2\min}) \tag{26}$$

where, f_{set} -particle target fitness, f_{avg} -particle average fitness, f -particle current fitness, k -current number of iterations, $k_{\max}$ -maximum number of iterations.

In order to avoid the stagnation state of particles, i.e., the velocity of the particle at the current moment is almost 0, the particle needs to be re-initialized with the position velocity. So set the particle stagnation record, and set a threshold, when the threshold is reached, the particle initialization. Specifically improve the PSO algorithm flow, as shown in Figure 2.

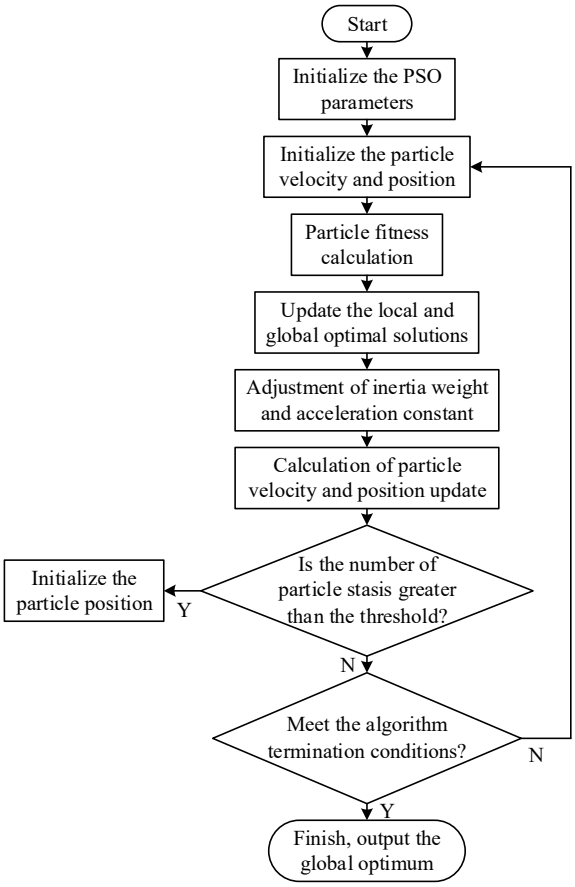

Figure 2: Flowchart of the improved PSO algorithm

III. Analysis of the regulation accuracy of the motorized bus frequency

III. A. Experimental verification of frequency regulation accuracy and analysis of test results

AD9956 is a high-precision DDS chip with 48-bit resolution capability, according to the formula FOUT=REFCLK*N/2^{48} (FOUT is the output frequency, REFCLK is the reference frequency, N is the frequency control word, and 48 is the number of frequency register bits). When taking N = 1, the calculation can be obtained AD9956 output signal frequency step accuracy of 3.5487E-15, according to the electric busbar synthesis circuit multiplier coefficient (about 684.4945) calculations, the theoretical 10MHz output signal frequency of the highest adjustment accuracy of 5.3123E-18, fully able to satisfy the application requirements of the busbar. Considering that the second stability index of the 10 MHz output signal of the busbar is at the level of 3.8E-12, it is impossible to accurately measure the change of its frequency accuracy by the test instrument when the frequency adjustment amplitude is too small. In order to verify the practical effect of the high-precision frequency regulation circuit scheme designed and implemented in this paper, the following set of comparative test experiments were done, and it can be seen through calculations that, when the amount of frequency control word change △N is set to 192315, the frequency of change is 192315 times the step value, and at this time, the amount of change in the accuracy of the 10 MHz output signal is 0.8E-12. By using the Picotime Frequency Stability Tester to test the 10 MHz output signal before and after the above frequency adjustment respectively, the data sampling interval is 1 s, the test sampling time is 100 s, the frequency accuracy of these 100 points is recorded, and the average value is calculated, and the frequency accuracy accuracy accuracy accuracy accuracy of the program is verified by comparing the deviation of the average value of the frequency accuracy before and after the frequency adjustment, the frequency accuracy test The results are shown in Fig. 3, Fig. (a) shows the frequency accuracy test results before frequency adjustment, and Fig. (b) shows the frequency accuracy test results after frequency adjustment.

Test and analysis of the calculation results show that the average value of the output frequency accuracy test results before frequency adjustment is -2.8787E-11, the average value of the frequency accuracy test results after frequency adjustment is -2.8191E-11, so the actual measured frequency Through the above experimental verification and test data analysis, it can be seen that when the amount of change is 192315 times the minimum step value, the output frequency accuracy can be realized in the 0.8E-12 order of magnitude of the precise adjustment. And it can be inferred from this, when the frequency control word change amount △ N is set to 1 (minimum step value), the program can realize the highest frequency regulation accuracy of 5.3123E-18.

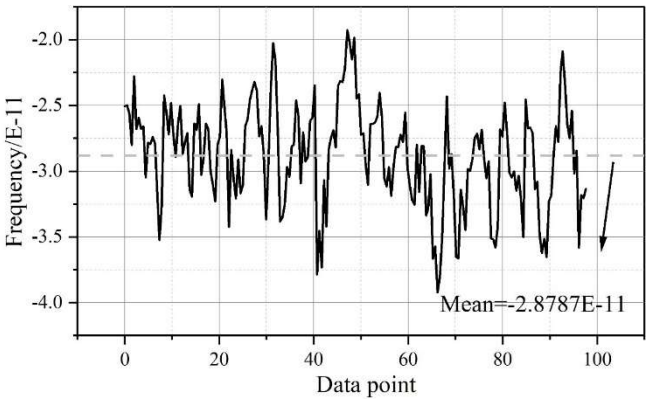

(a)Test results of the frequency accuracy of frequency adjustment

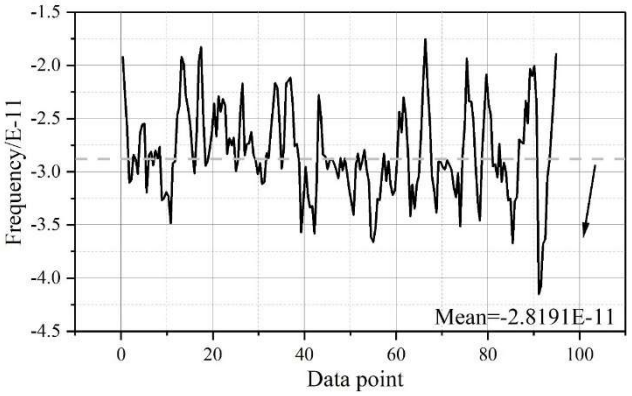

(b)Test results of frequency adjustment

Figure 3: Frequency adjustment accuracy test results

III. B. Analysis of the frequency regulation capability of the PSO-AFNIS model

III. B. 1) Parameter setting

Based on the model constructed in the previous section, the two-region interconnected system containing energy storage is designed for simulation in Matlab/Simulink platform, and the secondary FM of both region 1 and region 2 is completed by the conventional unit and four groups of BESS, and the system is standardized with the rated frequency of 60Hz and 600MW as the reference value (p.u.). The system parameters are set: the sampling time T of the DMPC controller is 0.15s, the prediction time domain Tp is 17s, the control time domain Tc is 8s, the convergence accuracy εD is taken as 0.15, and the new energy share ζ is 48%. Parameter settings of the units in each region: the rated capacity of the conventional unit is 1500 MW, and the FM capacity is -50~50 MW.

For the demand of multi-region secondary FM, the FM effect and distributed coordination capability are calibrated by the relevant parameters of two regions under different step perturbations.

III. B. 2) Motorized bus frequency regulation capability

For the demand of multi-region secondary FM, the FM effect and distributed coordination capability are calibrated by the relevant parameters of two regions under different step perturbations. At the same moment, a step perturbation with ΔP_L of 0.01 (p.u.) is added to region 1, and a step perturbation with ΔP_L of 0.015 (p.u.) is added to region 2, and the PSO-AFNIS (scheme 3), the centralized model predictive control without considering the coupling effect (scheme 2), and the PI control (scheme 1) of this paper are compared and analyzed.

In order to verify the effectiveness of this paper's strategy in terms of frequency regulation capability, the frequency deviation of each region under the three schemes, the regional control deviation ACE and the power change of the liaison line between regions are compared and analyzed. The simulation results are shown in Fig. 4 to Fig. 6.

Fig. 4 shows the frequency comparison of each region under the three schemes, and Figs. (a) and (b) show the comparison curves of frequency deviation under different step perturbations for region 1 and region 2, respectively: all three schemes are able to regulate the frequency deviation of region 1 and region 2 without any difference, and the net load perturbation in region 2 is smaller compared to that in region 1, which has less frequency deviation and less burden of frequency regulation. Under the combined comparison, the level of frequency deviation regulation of Scheme 3 is 56.8466% and 26.5412% higher than that of Scenarios 1 and 2 in Region 1, and the level of frequency deviation regulation of Scheme 3 is 40.1549% and 20.9816% higher than that of Scenarios 1 and 2 in Region 2. Therefore, Scheme 3 is able to recover the frequency deviation to zero in a shorter time, suppressing the frequency deviation fluctuation while improving the frequency recovery efficiency.

Fig. 5 shows the comparison of ACE in each region under the three schemes, and Figs. (a) and (b) show the comparison curves of ACE in region 1 and region 2 under different step perturbations, respectively: during the secondary FM process, the AGC generates the total FM out command which needs to switch the response to the ACE and the ARR signals, and therefore the ACE signals under the three schemes are not zero at the end of FM. Under the combined comparison, in region 1, the ACE regulation level of scheme 3 is improved by 50.5632% and 40.5391% compared with schemes 1 and 2, and in region 2, the ACE regulation level of scheme 3 is improved by 38.6423% and 27.6188% compared with schemes 1 and 2. In scheme 3, the regulation efficiency of the adaptive fuzzy control algorithm is significantly better than that of the CMPC controller and the PI controller, which can suppress the ACE to a smaller range at a faster rate and effectively reduce the amount of FM overshooting while improving the efficiency of the disturbance response in each region.

Fig. 6 shows the comparison of contact line power in each region, and Figs. (a) and (b) show the change curves of internal contact line power in region 1 and region 2, respectively: Scenarios 1 and 2 do not consider the support of contact line power between interconnected regions, and each region needs to mobilize a large amount of internal contact line power to participate in the regulation in the process of frequency restoration, so that the amplitude of the change in the internal contact line power in each region is larger and the time of the fluctuation is longer. Overall, the contact line power of scheme 2 is slightly lower than that of scheme 1, and the fluctuation ranges of the contact line power of scheme 2 in regions 1 and 2 are [-0.0075,0.0075], [-0.005,0.005], respectively.

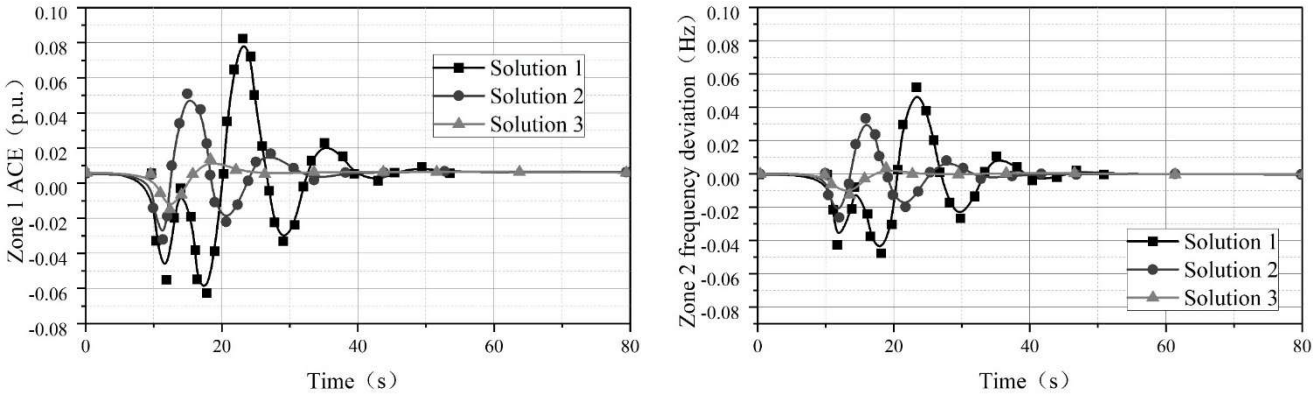

(a)Comparison of frequency deviation in Area 1 (b)Comparison of frequency deviation in Area 2

Figure 4: The frequency comparison of each area under the three schemes

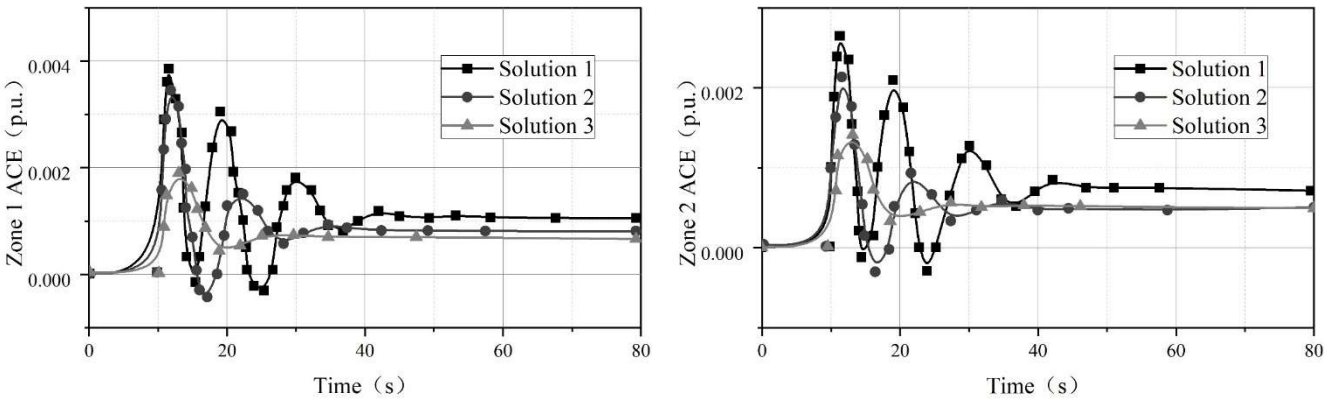

(a)The ACE comparison in Area 1 (b)The ACE comparison in Area 2

Figure 5: The comparison of ACE in each area under the three schemes

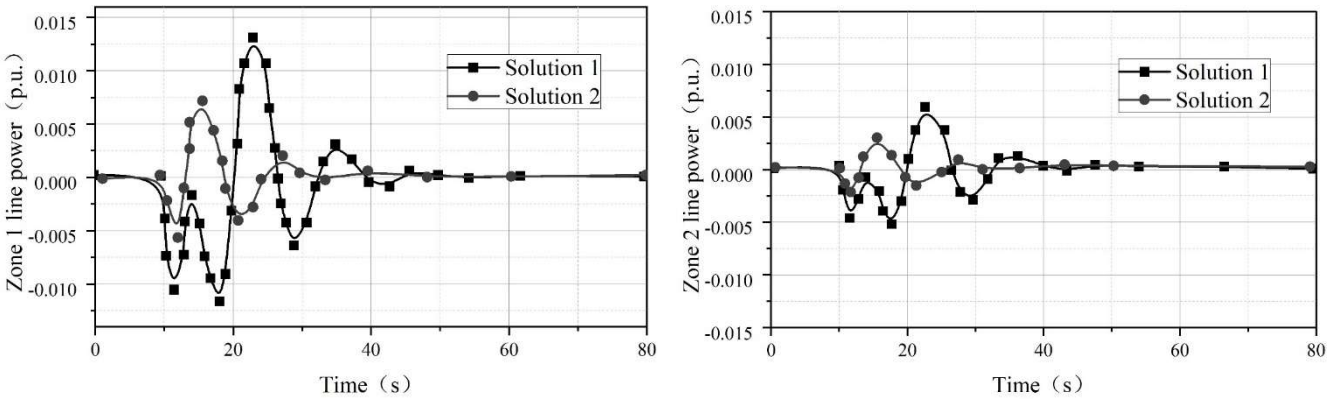

(a)The power comparison of the connecting lines in Area 1 (b)The power comparison of the connecting lines in Area 2

Figure 6: The power comparison of the connecting lines in each area under

III. B. 3) Coordination capacity

A 5% ($\Delta P_{L,1}$=0.06p.u.) step disturbance is considered in region 1, and the simulation results are shown in Fig. 7, Fig. (a) shows the comparison of frequency deviation in region 1, Fig. (b) shows the comparison of frequency deviation in region 2, and Fig. (c) shows the comparison of power deviation of the liaison line in regions under different scenarios.In order to validate the effect of different kinds of electric bus clusters participating in FM together with this paper's control strategy, the comparison of the The system frequency deviation of fixed-frequency electric bus and variable-frequency electric bus participating in FM together with that of both participating in FM alone.

In order to verify the effectiveness of the coordinated control strategy proposed in this paper, the following four scenarios are set up for simulation and analysis.

Scenario 1: Only the generator participates in FM.

Scenario 2: ANFIS participates in the electric bus frequency control and the FM power is shared by generator and ANFIS.

Scenario 3: PSO participates in electric bus frequency control, FM power is shared by generator and PSO.

Scenario 4: (the strategy proposed in this paper): PSO and ANFIS participate in electric bus frequency control collaboratively, and the FM power is shared by the generator, PSO and ANFIS.

The maximum frequency deviation when PSO and AFNIS are jointly involved in FM in region 1 is -0.1236 Hz, and the maximum frequency deviation when each of the two motorized busbars is individually involved in FM is -0.1698 Hz and -0.1628 Hz, respectively, i.e., the PSO and AFNIS are jointly involved in FM to better cut down the amount of frequency deviation. Similarly, the maximum frequency deviation is 37.6485% less when PSO and AFNIS are jointly involved in FM than when only AFNIS is involved in FM in region 2 in Fig. 7(b), and 31.5697% less when PSO is only involved in FM. It can be seen that the system frequency recovery is faster, the recovery time is shorter, and the frequency overshoot is more slight when fixed-frequency and variable-frequency are jointly involved in FM. In addition, the power deviation of the contact line in three cases is 0.0267 p.u., 0.0359 p.u. and 0.0319 p.u.

respectively, which means that the power deviation of the contact line is the smallest when fixed-frequency and inverter participate in FM, and the contact line fluctuation can be effectively suppressed. It can be seen that coordinating the participation of fixed-frequency electric bus and variable-frequency electric bus loads in frequency regulation can improve the frequency regulation performance of the system, and also make full use of the flexibility of the two types of flexible loads to mobilize more demand-side flexibility resources.

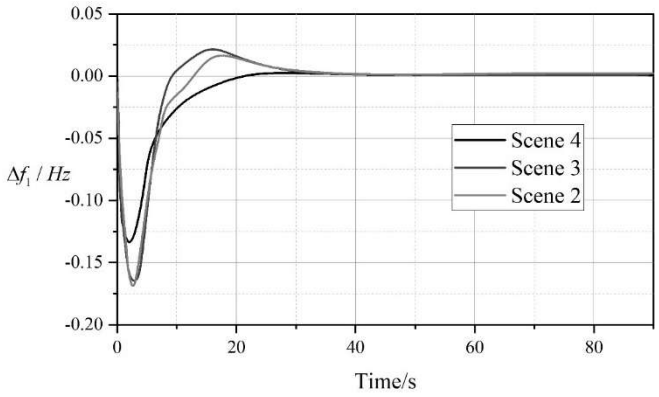

(a)The frequency deviation of area 1 is compared

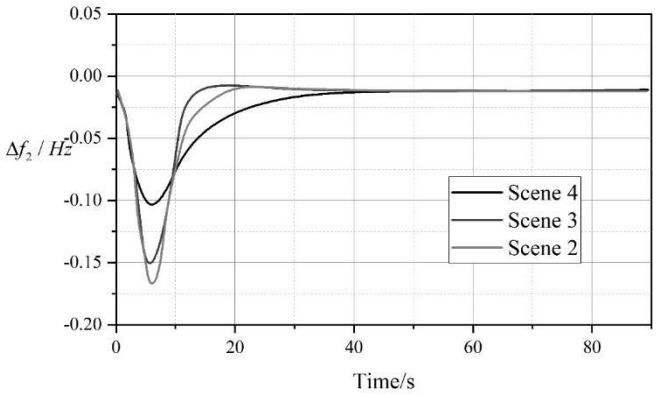

(b)Region 2 frequency deviation

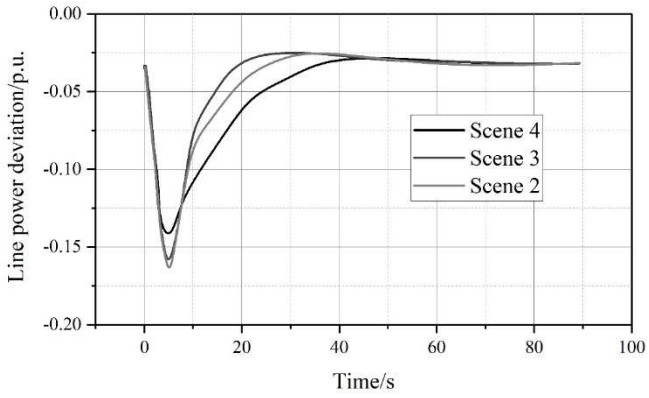

(c)Contrast of the line power deviation of the contact line in the region under different scenarios

Figure 7: Effects of multi-region and single-region frequency modulation strategies

IV. Conclusion

The electric bus frequency regulation scheme based on adaptive fuzzy control algorithm significantly improves the regulation accuracy and stability of the system. Experimental validation shows that the scheme can realize the highest frequency regulation accuracy of 5.3123E-18, which meets the practical application requirements of electric busbar. The results of multi-region simulation and analysis show that the frequency deviation regulation level of PSO-ANFIS control strategy in region 2 is improved by 40.15% and 20.98% compared with the traditional PI control and centralized model prediction control, respectively. Meanwhile, in terms of area control deviation (ACE) regulation, the PSO-ANFIS strategy improves the regulation level in area 2 by 38.64% and 27.62% compared with the PI control and centralized model prediction control, which effectively reduces the amount of overshooting in the frequency regulation and enhances the efficiency of perturbation response. When the fixed-frequency and variable-frequency electric buses participate in frequency regulation, the system contact line power deviation is reduced to 0.0267 p.u., which is 16.30% and 25.63% less than that of using PSO or ANFIS alone, respectively, and the power fluctuation of the contact line is significantly smoothed. In addition, under the 5% step disturbance condition, the cooperative strategy can control the maximum frequency deviation of the system at -0.1236 Hz, which is reduced by 27.21% and 24.08% compared with the application of PSO or ANFIS strategy alone, respectively. These results fully demonstrate the significant advantages of the proposed adaptive fuzzy control algorithm in improving the frequency regulation accuracy of the electric bus, accelerating the frequency recovery speed, reducing the FM overshooting amount, and coordinating the power fluctuation of the contact line of the multiregional power system,

which provides a new way of thinking for the further development of the frequency control technology of the power system.

References

[1] Liu, Z., Hao, H., Cheng, X., & Zhao, F. (2018). Critical issues of energy efficient and new energy vehicles development in China. Energy Policy, 115, 92-97.

[2] Tan, L., Zhang, W., & Zhang, F. (2019). Research on energy efficiency system of new energy vehicle electric drive. In IOP Conference Series: Earth and Environmental Science (Vol. 223, No. 1, p. 012028). IOP Publishing.

[3] RATHORE, Vinay, et al. A high-gain multilevel dc–dc converter for interfacing electric vehicle battery and inverter. IEEE Transactions on Industry Applications, 2022, 58.5: 6506-6518.

[4] LIN, Gang, et al. Inertia droop control and stability mechanism analysis of energy storage systems for dc-busbar electric vehicle charging station. IEEE Transactions on Transportation Electrification, 2022, 9.1: 266-282.

[5] Migliazza, G., Buticchi, G., Carfagna, E., Lorenzani, E., Madonna, V., Giangrande, P., & Galea, M. (2020). DC current control for a single-stage current source inverter in motor drive application. IEEE Transactions on Power Electronics, 36(3), 3367-3376.

[6] Alizadeh, R., Schupbach, M., Adamson, T., Balda, J. C., Zhao, Y., Long, S., ... & Goodson, K. E. (2018, September). Busbar design for distributed DC-link capacitor banks for traction applications. In 2018 IEEE Energy Conversion Congress and Exposition (ECCE) (pp. 4810-4815). IEEE.

[7] Roh, C., Jeon, H. M., Kim, S. W., Kim, J. S., Song, S. W., Lee, N. Y., & Kang, S. C. (2025). A Study on Equivalent Series Resistance Estimation Compensation for DC-Link Capacitor Life Diagnosis of Propulsion Drive in Electric Propulsion Ship. Processes, 13(2), 291.

[8] De Angelis, A., Carbone, P., Santoni, F., Vitelli, M., & Ruscitti, L. (2023). On the Usage of Battery Equivalent Series Resistance for Shuntless Coulomb Counting and SOC Estimation. Batteries, 9(6), 286.

[9] Burcea, I. M., Svasta, P., & Negroiu, R. (2023, May). The Influence of the Equivalent Series Resistance (ESR) on the Functional Behaviour of Electrochemical Double Layer Capacitors (EDLCs). In 2023 46th International Spring Seminar on Electronics Technology (ISSE) (pp. 1-5). IEEE.

[10] Rodes, F., & Hochart, X. (2023). Improvement of the Standard Test Method for Effective Series Resistance (ESR) and Capacitance of Ultra High-Q Capacitors at High Frequencies. IEEE Instrumentation & Measurement Magazine, 26(6), 28-31.

[11] Wang, K., Lu, H., Chen, C., & Xiong, Y. (2022). Modeling of system-level conducted EMI of the high-voltage electric drive system in electric vehicles. IEEE Transacti1ons on Electromagnetic Compatibility, 64(3), 741-749.

[12] Ripka, P., Grim, V., & Petrucha, V. (2016). A busbar current sensor with frequency compensation. IEEE Transactions on Magnetics, 53(4), 1-5.

[13] Bhukya, C. N., & Reddy, B. A. (2023, September). Constant power loads in dc microgrids: A review of modern nonlinear control approaches and stabilisation techniques. In 2023 IEEE 2nd international conference on industrial electronics: Developments & applications (ICIDeA) (pp. 181-186). IEEE.

[14] He, W., Namazi, M. M., Koofigar, H. R., Amirian, M. A., & Guerrero, J. M. (2021). Voltage regulation of buck converter with constant power load: An adaptive power shaping control. Control Engineering Practice, 115, 104891.

[15] Hassan, M. A., Worku, M. Y., Eladl, A. A., Elkadeem, M. R., Hossain, M. I., & Abido, M. A. (2024). Instability Mitigation of Constant Power Load in Microgrid. Arabian Journal for Science and Engineering, 49(5), 7341-7358.

[16] Fu, Q., Du, W., Wang, H., & Xiao, X. (2022). Effect of the dynamics of the MTDC power system on DC voltage oscillation stability. IEEE Transactions on Power Systems, 37(5), 3482-3494.

[17] Fu, Q., Du, W., Wang, H., Ma, X., & Xiao, X. (2022). DC voltage oscillation stability analysis of DC-voltage-droop-controlled multiterminal DC distribution system using reduced-order modal calculation. IEEE Transactions on Smart Grid, 13(6), 4327-4339.

[18] Sun, Z., Han, Y., Wang, Z., Chen, Y., Liu, P., Qin, Z., ... & Song, C. (2022). Detection of voltage fault in the battery system of electric vehicles using statistical analysis. Applied Energy, 307, 118172.

[19] Yusuf H & Ahkadun N. (2021). Analysis of Effect Electric Field Strenght on Safe Distance Below Main Substation Busbar 150 kV. Journal of Physics: Conference Series,1764(1),012170-.

[20] Krishna Kumar,Madhulika Das & Amrendra Kumar Karn. (2024). ANFIS robust control application and analysis for load frequency control with nonlinearity. Journal of Electrical Systems and Information Technology,11(1),65-65.

[21] Labed Nasreddine,Attoui Issam,Makhloufi Salim,Bouraiou Ahmed & Bouakkaz Mohammed Salah. (2022). PSO Based Fractional Order PI Controller and ANFIS Algorithm for Wind Turbine System Control and Diagnosis. Journal of Electrical Engineering & Technology,18(3),2457-2468.